Stability of Mn moments and exchange interactions in cobalt substituted Mn_2Sb

2008 J. Phys.: Condens. Matter 20 015220

(http://iopscience.iop.org/0953-8984/20/1/015220)

J. Phys.: Condens. Matter **20** (2008) 015220 (7pp) doi:10.1088/0953-8984/20/01/015220

Stability of Mn moments and exchange interactions in cobalt substituted Mn_2Sb

P J Brown[1,2], A P Gandy[1], T Kanomata[3] and K R A Ziebeck[1]

[1] Department of Physics, Loughborough University, LE11 3TU, UK
[2] Institut Laue-Langevin, BP 156, 38042 Grenoble, France
[3] Faculty of Engineering, Tohoku Gakuin University, Tagajo 985-8537, Japan

Received 19 October 2007, in final form 14 November 2007
Published 7 December 2007
Online at stacks.iop.org/JPhysCM/20/015220

Abstract

The magnetic moment distributions in the ferrimagnetic (FI) and antiferromagnetic (AF) phases of Co substituted Mn_2Sb ($Mn_{1.9}Co_{0.1}Sb$) have been determined using both polarized and unpolarized neutron diffraction. In $Mn_{1.9}Co_{0.1}Sb$ a transition from a ferrimagnetic to an antiferromagnetic state takes place on cooling through $T_{ms} = 138$ K. The antiferromagnetic structure has propagation vector $(00\frac{1}{2})$, and contains (001) layers of Mn atoms with ferromagnetically coupled Mn moments aligned perpendicular to [001]. The two crystallographically distinct Mn atoms have moments 3.98 and 1.71 μ_B at 4 K and are oppositely aligned within the unit cell. At 200 K the moments determined from polarized neutron scattering are 3.86 and 1.84 μ_B. In both the AF and FI phases the magnetization associated with the high moment (Mn2) site is nearly spherically symmetric; that around the Mn1 site has predominantly t_{2g} character which is stronger in the AF than in the FI phase. At T_{ms} the only bonds whose lengths change significantly are those between Mn and Sb establishing the 125° Mn1–Sb–Mn2 interlayer exchange path as the dominant exchange interaction determining the type of long range magnetic order.

(Some figures in this article are in colour only in the electronic version)

1. Introduction

Mn_2Sb crystallizes with the tetragonal C38 structure, space group $P4/nmm$. It contains two crystallographically distinct Mn sites: 2(a) Mn1 with symmetry $\bar{4}2m$ and 2(c) Mn2 with symmetry $4mm$. In the pure phase the Mn magnetic moments order ferrimagnetically below 550 K. and at 5 K the Mn1 and Mn2 sites have oppositely orientated moments of 2.1 and 3.9 μ_B [1]. Above $T_{sf} = 240$ K the moments are parallel to the c axis and below it they lie in the (001) plane. Mn can be replaced by Co in the structure up to a limit of ≈17 at.% and in alloys $Mn_{2-x}Co_xSb$ with $0.1 < x < 0.35$ there is a first order phase transition at temperatures around $T_{ms} = 180$ K in which the magnetic structure changes from the ferrimagnetic Mn_2Sb (FI) to the antiferromagnetic Mn_2As type (AF). There is no change in crystal structure associated with the magnetic transition although it is accompanied by an abrupt 0.4% decrease in the length of the c-axis [2] leading to a discontinuous reduction in $\Delta V/V$ of only $\approx 5 \times 10^{-4}$ in unit cell volume [4]. It has been reported that there is also an anomalous increase in the magnetic moment of the Mn2 atom at the transition [3].

Spin polarized band structure calculations have been made for ferrimagnetic Mn_2Sb by Suzuki *et al* [5] and for Mn_2Sb in ferromagnetic, ferrimagnetic and antiferromagnetic states by Wjingaard *et al* [6]. The two calculations give very similar results for the ferrimagnetic phase. They show rather narrow and well separated up and down spin 3d bands for the Mn2 atoms. Those associated with Mn1 atoms are much broader and overlap strongly. Comparison of the results for the FI and AF calculations [6] shows narrowing of the Mn2 3d bands in the AF state and significant changes leading to sharper peaks, near to the Fermi surface, in the density of states associated with Mn1 atoms. No information about the symmetry of the functions contributing to the density of states is given. The greater width of the Mn1, relative to the Mn2 3d band obtained in the APW calculations for paramagnetic Mn_2Sb is consistent with photoemission and inverse photoemission experiments [7]. These band structure calculations indicate that the 3d electrons associated with Mn atoms have an itinerant character with the Fermi level lying between a two peak structure in the density of states. With this form of DOS the electronic structure, on which the magnetic order depends, is highly sensitive to the d-electron concentration and may alter

significantly when Co replaces Mn. An electronic origin for the AF–FI transition in $Mn_{2-x}Co_xSb$ ($x = 0.18$) is also indicated by specific heat measurements. The electronic Sommerfeld contribution to the specific heat increases by ≈39% at the critical field for the field induced AF–FI transition due to an increase in the DOS at the Fermi energy [8, 9]. This increase also leads to an abrupt decrease in electrical resistivity in the AF–FI transition making the material of potential use as a thermal switch.

Previous neutron diffraction measurements on $Mn_{2-x}Co_x$ Sb ($x = 0.2$) with $T_{ms} = 170$ K and $T_C = 400$ K suggest that the cobalt atoms replace Mn atoms in the Mn1 2(a) sites only. The moments on the Mn1 and Mn2 sites were found to be 0.98 and 1.86 μ_B respectively at room temperature, rising to 1.77 and 3.47 μ_B in the AF phase at 78 K. The increase in the Mn1 moment is consistent with that expected for an $S = \frac{1}{2}$ Brillouin function, whereas the change in the Mn2 moment suggests an abrupt increase by approximately 1 μ_B at T_{ms} [3]. Since there is continuing interest in the stability of Mn moments in metallic compounds, this anomalous change at the AF–FI transition of just one of the Mn moments in $Mn_{2-x}Co_xSb$ makes it an attractive system for further study. We have therefore undertaken an investigation the of crystal structure and magnetization distribution of a single crystal of $Mn_{2-x}Co_xSb$ ($x = 0.1$), as a function of temperature to clarify the precise nature of the magnetic transition and any accompanying anomalous change in the magnetic moments.

2. Experimental details

2.1. Sample preparation

A polycrystalline sample of $Mn_{1.9}Co_{0.1}Sb$ was prepared from powders of cobalt, manganese and antimony all with 99.9% purity. They were mixed in the desired proportions, sealed in an evacuated silica tube and heated at 850 °C for 2 days. The temperature was then lowered to 600 °C and the sample was left for one day before being quenched into water. A single crystal was grown from the polycrystalline ingot using the Bridgman method. The experiment was carried out on a piece cut from this crystal 4.6 × 1.5 × 1.1 mm^3 elongated parallel to [110] and with its shortest axis parallel to [001].

2.2. Magnetization measurements

Magnetization measurements were made using a SQUID magnetometer in fields up to 5.5 T and at stable temperatures between 5 and 350 K. The magnetic moments per unit cell derived from these measurements are plotted as filled circles in figure 1.

2.3. Unpolarized neutron measurements

The crystal was mounted in the He flow cryostat of the 4-circle diffractometer D10 at ILL Grenoble. After determining the orientation it was cooled from 200 to 80 K in steps of 2 K and from 80 to 4 K in steps of 4 K. At each step the integrated intensities at the positions of the 002 and $00\frac{1}{2}$ reflections were measured. Below 138 K the intensity of the 002 reflection

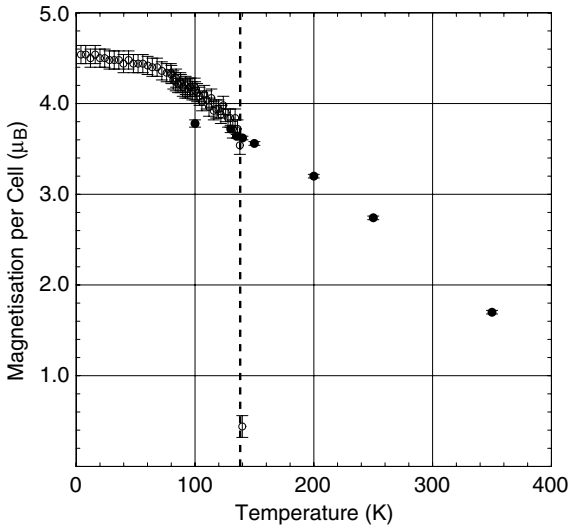

Figure 1. Temperature dependence of the unit cell magnetization in $Mn_{1.9}Co_{0.1}Sb$. The points marked ● were derived from the magnetization measurements and the ○ show the variation of the sublattice magnetization in the AF phase derived from the intensity measurements of figure 2. The vertical dashed line indicates T_{ms}.

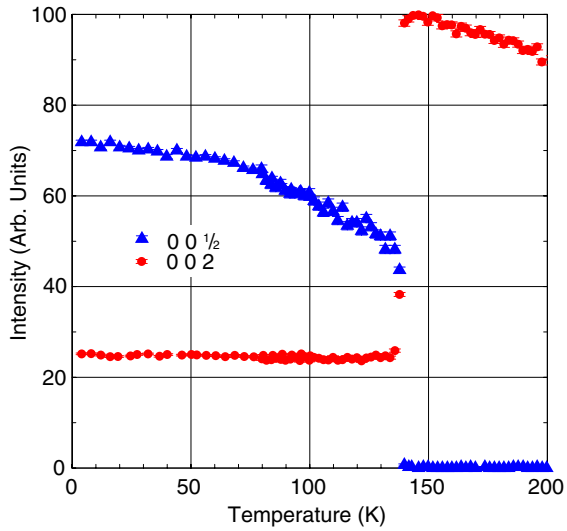

Figure 2. Temperature dependence of the integrated intensities of the 002 and $00\frac{1}{2}$ reflections of $Mn_{1.9}Co_{0.1}Sb$. At $T_{ms} = 138$ K the magnetic structure changes from ferrimagnetic to antiferromagnetic with propagation vector $(00\frac{1}{2})$.

diminished sharply and intensity appeared at the position of $00\frac{1}{2}$ as shown in figure 2. This confirms the transition from the ferrimagnetic Mn_2Sb structure to an antiferromagnetic one with propagation vector $(00\frac{1}{2})$. The temperature, 138 K, at which the transition occurs is that given by the composition dependence of T_{ms} determined by [2] for a cobalt content of 5(2) at.%.

The integrated intensities of all the accessible magnetic and nuclear reflections with $\sin\theta/\lambda < 0.4$ $Å^{-1}$ were measured at 4 K with a neutron wavelength of 2.353 Å. The set of nuclear reflections was remeasured at 160 K. With a shorter

Table 1. Parameters obtained from the structure refinements of $Mn_{1.9}Co_{0.1}Sb$ at 160 K.

Space group $P4/nmm$ $a = 4.0648(13)$ Å $c = 6.391(4)$ Å								
	Isotropic refinement				Anisotropic refinement			
Site	Co%	z	B (Å^2)	μ (μ_B)	Co%	z	B_{ij} [a]	μ (μ_B)
Mn1 2(a) ($\frac{1}{4}\frac{3}{4}0$)	8(2)		1.2(2)	−1.75(11)	11(2)		0.9(2) 0.9(2)	−2.22(13)
Mn2 2(c) ($\frac{1}{4}\frac{1}{4}z$)	0	0.2900(6)	1.2(2)	3.65(13)	0	0.2904(5)	0.8(2) 1.7(2)	3.80(12)
Sb 2(c) ($\frac{1}{4}\frac{1}{4}z$)	0	0.7220(5)	1.0(1)		0	0.7222(4)	0.5(1) 1.6(1)	
χ^2			31				19	
R_{cryst}			6.5				5.2	

[a] For each pair of values the upper is B_{11} and the lower B_{33}, the units are Å^2.

Table 2. Parameters obtained from the structure refinements of $Mn_{1.9}Co_{0.1}Sb$ at 4 K.

Space group $P4/nmm$ $a = 4.0681(13)$ Å $c = 6.394(3)$ Å								
	Isotropic refinement				Anisotropic refinement			
Site	Co%	z	B (Å^2)	μ (μ_B)	Co%	z	B_{ij} [a]	μ (μ_B)
Mn1 2(a) ($\frac{1}{4}\frac{3}{4}0$)	10.5(9)		0.7(1)	−1.80(6)	11(2)		0.7(1) 0.9(1)	−1.71(4)
Mn2 2(c) ($\frac{1}{4}\frac{1}{4}z$)	0	0.2914(6)	1.3(1)	4.33(8)	0	0.2912(6)	0.8(1) 1.7(2)	3.98(6)
Sb 2(c) ($\frac{1}{4}\frac{1}{4}z$)	0	0.7233(4)	1.0(1)		0	0.7236(3)	0.6(1) 1.6(1)	
χ^2			21				16	
R_{cryst}			6.3				4.9	

[a] For each pair of values the upper is B_{11} and the lower B_{33}, the units are Å^2.

wavelength: 1.53 Å a further set of 83 independent nuclear reflections with $\sin\theta/\lambda < 0.61$ Å^{-1} was measured at 160 K and at 4 K. Finally a few magnetic reflections were also measured at the shorter wavelength to confirm the scaling of the magnetic moments.

Refinements of the nuclear structure were carried out using the data collected at 160 K and at 4 K. Initial refinements gave the ratio between the scattering lengths at the Mn and Sb 2(c) sites as −0.71(3). This shows that these two sites must be completely occupied by Mn and Sb respectively; any Co atoms in either of the sites would reduce the absolute value of the ratio from its maximum for full occupation of 0.67. It was therefore assumed in the subsequent refinements that there is no Co in either the Mn2 or Sb sites. In the 160 K refinement of the FI structure magnetic moments were determined for the two transition metal sites. For the 4 K data the magnetic structure was refined separately using the data with half integral l with the scale factor, extinction parameter and Mn structure parameters obtained in the nuclear refinement. In the magnetic structure the moments of Mn atoms in layers with constant z are ferromagnetically coupled and aligned perpendicular to [001]. Adjacent Mn1 and Mn2 layers are antiferromagnetically coupled.

The results of the refinements using the 160 K data are given in table 1 and those for the 4 K data in table 2. It can be seen from these tables that a very significant improvement in the goodness of fit is obtained by including anisotropic thermal vibration. The values B_{33} which characterize displacements along the c-axis, are very much larger than those of B_{11} which depend on displacements perpendicular to it. The anisotropy is particularly marked at both sets of 2(c) sites and the values of B_{33} are not much smaller at 4 K than at 160 K. This suggests that they probably arise from static displacements associated with atomic disorder, rather than from true thermal motion. The percentage of cobalt in the 2(a) sites was not significantly different from 10 in any of the refinements, in good agreement with both the nominal composition and that estimated from T_{ms}.

Table 3. Parameters determined for different models of the magnetization distribution in the FI phase of $Mn_{1.9}Co_{0.1}Sb$ at 200 K.

	Spherical models moments (μ_B)			Multipole models coefficients (μ_B)		
Site	(a)	(b)		(c)	(d)	(e)
Mn1	−1.721(19)	−2.28(14)	Y_0^0	−1.84(2)	−2.16(14)	−2.21(13)
			Y_2^0	0.00(3)	−0.02(3)	−0.03(3)
			Y_4^0	0.07(5)	0.08(5)	−0.04(5)
			$(Y_4^4 + Y_4^{-4})/\sqrt{2}$	−0.16(6)	−0.16(3)	0.17(7)
Co1		0.57(12)			0.28(12)	0.32(11)
Mn2	3.264(17)	3.287(16)	Y_0^0	3.45(2)	3.46(2)	3.46(2)
			Y_2^0	0.01(3)	0.00(3)	0.00(2)
			Y_3^0			−0.08(2)
			Y_4^0	0.04(6)	0.04(6)	0.05(5)
			$(Y_4^4 + Y_4^{-4})/\sqrt{2}$	0.04(7)	−0.03(7)	0.02(7)
χ^2	6.3	5.0		4.5	4.2	3.8

2.4. Polarized neutron measurements

The magnetic contribution to the structure factors in the FI phase of $Mn_{1.9}Co_{0.1}Sb$ has been determined from measurements of the polarization dependence of the intensities of the Bragg peaks at 200 K. The same crystal was used as for the integrated intensity measurements. It was mounted on the polarized neutron diffractometer D3 at ILL Grenoble, first with $[1\bar{1}0]$ and then with [010], approximately parallel to the magnetizing field of 8 T. With the normal beam geometry of the D3 diffractometer and a wavelength of 0.843 Å reflections in the zero, first and second layers were accessible in both orientations; 213 reflections were measured with the first and 58 with the second.

The initial analysis was carried out using a simple model consisting of spherically symmetrical manganese moments which were fitted to the measured asymmetries A_p in the reflection intensities.

$$A_p = (I^+ - I^-)/(I^+ + I^-)$$

where I^+ and I^- are the intensities scattered with the polarization, respectively, parallel and antiparallel to the magnetization direction. In this analysis all the reflections measured are treated independently and the method allows the polarizing efficiency to be refined. The nuclear positions and temperature factors used for the model were those determined from the integrated intensity measurements at 160 K. The refinement gave −1.92(2) and 3.39(2) μ_B for the moments at the Mn1 and Mn2 sites respectively and 0.871(3) and 0.891(3) as the effective polarizing efficiencies for the two data sets. Using these polarizing efficiencies and the same nuclear parameters the magnetic structure factor corresponding to each flipping ratio measurement was calculated. After averaging over equivalents and merging the two sets of data, a set containing magnetic structure factors for 83 independent *hkl* was obtained.

The degree to which the spherical model fails to fit the measured data can be displayed in real space by making a maximum entropy reconstruction of the difference between the magnetization distribution of the spherically symmetric model and that corresponding to the measured data. A section of this reconstruction parallel to (010) at $x = 0.25$, which passes through all the atoms, is shown in figure 3. The significant features on the map are a small positive peak associated with Mn1 and a negative area around the Sb site. There is a gradient at the Mn2 site showing that the centre of gravity of the magnetization is shifted towards its nearest Sb neighbour (that with $z = 0.72$) just as was found in pure Mn_2Sb [10].

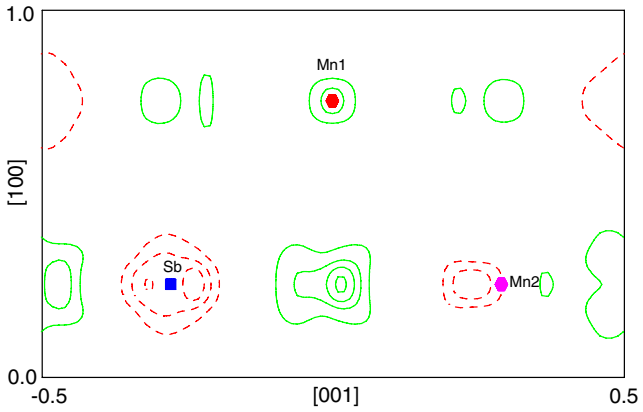

Figure 3. Maximum entropy reconstruction of the difference between the observed magnetization distribution in $Mn_{1.9}Co_{0.1}Sb$ and that calculated for a model made from spherically symmetric manganese 3d moments of −1.93 and 3.38 μ_B at the Mn1 and Mn2 sites, respectively. The section shown is parallel to (010) at height 0.25, the contours are at equal intervals of 0.1 μ_B Å^{-3}.

3. Modelling the magnetization distribution

Least squares fits of several different models for the magnetization distribution have been made to the magnetic structure factor data obtained for both the FI and AF phases. The results are summarized in tables 3 and 4. Model (a) in table 3 is the simple spherical model described previously. In (b) the Mn1 site magnetization is modelled by one given by a mixture of the Mn and Co neutral free atom form factors.

Table 4. Parameters determined for different models of the magnetization distribution in the AF phase of $Mn_{1.9}Co_{0.1}Sb$ at 4 K.

	Spherical models moments (μ_B)		Multipole models coefficients (μ_B)	
Site	(a)		(c)	(f)
Mn1	−1.37(3)	Y_0^0	−1.49(3)	−1.48(3)
		Y_2^0	−0.17(10)	−0.16(10)
		Y_4^0	−0.4(3)	−0.5(3)
		$(Y_4^4 + Y_4^{-4})/\sqrt{2}$	0.6(4)	0.7(4)
Mn2	3.98(5)	Y_0^0	4.14(5)	4.13(5)
		Y_2^0	0.19(14)	0.21(14)
		Y_3^0		−0.19(15)
		Y_4^0	0.0(5)	−0.2(5)
		$(Y_4^4 + Y_4^{-4})/\sqrt{2}$	0.3(4)	0.4(4)
χ^2	35		20.0	19.6

In (c) and (d) the magnetization distributions around the two Mn sites are described by a sum of symmetry compatible spherical harmonic functions of even order up to 4. The amplitudes of these functions were fitted to the data. For (e) in table 3 and (f) in table 4 the odd order harmonic Y_3^0 was added to model the gradient of magnetization observed at the Mn2 site in figure 3. For (c) only Mn form factors are used whereas (d) and (e) allow a spherical Co contribution at the Mn1 site. It can be seen from table 3 that the fits are improved by including an independent cobalt moment and the result suggests that it is oppositely orientated to the Mn moments on the same sites. However the Mn1 and Co moments obtained are highly correlated because there is only a small difference between the Mn and Co form factors. The precision and range in $\sin\theta/\lambda$ of the magnetic structure factors obtained from integrated intensity measurements in the AF phase is considerably less than that obtained from the polarized neutron measurements in the FI phase and did not permit the Mn1 and Co moments to be refined separately. Nevertheless the residual χ^2 values were reduced by including aspherical components in the magnetization distribution. The amplitudes listed in tables 3 and 4 refer to the site moments; for models (d) and (e): the moments on the Mn atoms at the Mn1 sites are −2.8(2) and −2.7(2) μ_B and that on the Co atoms 2.8(6) and 1.4(6) μ_B respectively.

The point group symmetries of the Mn1 and Mn2 sites in $Mn_{1.9}Co_{0.1}Sb$ are $\bar{4}2m$ and $4mm$ respectively. d functions with either of these point groups have three one-dimensional irreducible representations given by the combinations:

$$d_{3z^2-r^2} = |2,0\rangle; \qquad d_{x^2-y^2} = \frac{1}{\sqrt{2}}(|2,2\rangle + |2,-2\rangle);$$
$$d_{xy} = \frac{\iota}{\sqrt{2}}(|2,2\rangle - |2,-2\rangle)$$

and a single two-dimensional representation given by the functions

$$d(xz) = \frac{1}{\sqrt{2}}(|2,1\rangle + |2,-1\rangle) \qquad \text{and}$$

$$d(yz) = \frac{\iota}{\sqrt{2}}(|2,1\rangle - |2,-2\rangle).$$

The magnetization due to unpaired d electrons with these symmetries is proportional to the products of these functions with their complex conjugates:

$$|d_{3z^2-r^2}|^2 \propto \left(Y_0^0 + \frac{2\sqrt{5}}{7}Y_2^0 + \frac{6}{7}Y_4^0\right)$$

$$|d_{x^2-y^2}|^2 \propto \left(Y_0^0 - \frac{2\sqrt{5}}{7}Y_2^0 + \frac{1}{7}Y_4^0 + \sqrt{\frac{5}{14}}(Y_4^4 + Y_4^{-4})\right)$$

$$|d_{xy}|^2 \propto \left(Y_0^0 - \frac{2\sqrt{5}}{7}Y_2^0 + \frac{1}{7}Y_4^0 - \sqrt{\frac{5}{14}}(Y_4^4 + Y_4^{-4})\right)$$

$$|d_{xz}|^2 + |d_{yz}|^2 \propto \left(2Y_0^0 + \frac{2\sqrt{5}}{7}Y_2^0 - \frac{8}{7}Y_4^0\right).$$

These relationships allow the fractions of unpaired electrons in each of the non-degenerate 3d orbitals associated with the two manganese sites to be calculated from the multipole amplitudes listed in tables 3 and 4. The values obtained are given in table 5. Note that the orientation of the octahedral coordination polyhedron around the Mn1 atom is rotated by $\pi/4$ with respect to the conventional orientation in a cubic structure. The e_g-like functions therefore contain the xy, rather than the $x^2 - y^2$ orbitals. The odd order spherical harmonic Y_3^0 which is compatible with the point group symmetry $4mm$ and was included in fits to the magnetization distribution around the Mn2 site can arise from hybridization between $4p_z$ and $3d_{3z^2-r^2}$ orbitals. The value obtained for the FI phase corresponds to 7(2)% hybridization. A Brillouin function with $S = \frac{1}{2}$ and $T_C = 457$ K [2] has been used to estimate the moments corresponding to 0 K; the extrapolations are shown in figure 4.

Table 5. Magnetic moments and percentages of the unpaired electrons in each of the four non-degenerate 3d orbitals in $Mn_{1.9}Co_{0.1}Sb$ at 4 K(AF phase) and at 200 K (FI phase).

		Mn1		Mn2	
		AF	FI	AF	FI
Moment (μ_B)	Measured	−1.48(4)	−1.84(2)	4.01(5)	3.45(2)
	Extrapolated 0 K	−1.48(4)	−1.90(7)	4.01(5)	3.55(7)
Orbital	$d(3z^2 - r^2)$	0(12)	18(2)	21(7)	21(1)
	$d(x^2 - y^2)$	46(15)	27(1)	18(7)	21(1)
	$d(xy)$	0(15)	12(2)	17(7)	19(1)
	$d(xz)$, $d(yz)$	54(16)	43(2)	44(10)	39(1)

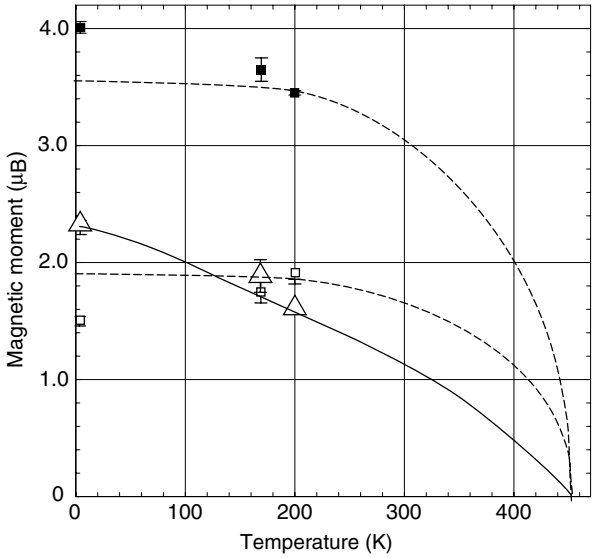

Figure 4. Magnetic moments at the Mn1 (□) and Mn2 (■) sites in $Mn_{1.9}Co_{0.1}Sb$. The △ show the total moments per formula unit derived from refinements of the diffraction data. The dashed curves are Brillouin function for $S = \frac{1}{2}$ and $T_C = 457$ K, scaled to pass through the Mn1 and Mn2 moments at 200 K. The full curve indicates the evolution of the magnetization with temperature derived from figure 1.

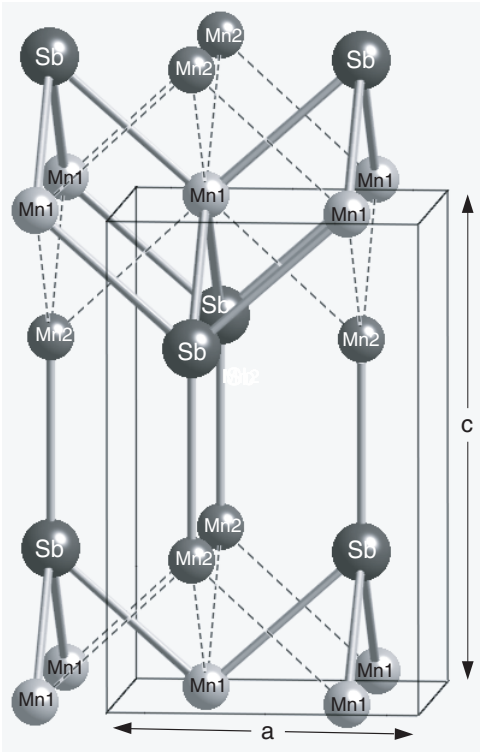

Figure 5. Schematic drawing of the structure of $Mn_{1.9}Co_{0.1}Sb$ showing all bonds less than 2.8 Å in length. The bonds which lengthen in the FI to AF transition are shown as solid rods whilst those which decrease slightly are shown as dashed lines.

4. Discussion

Figure 5 shows the crystal structure of Mn_2Sb with all the bonds of less than 2.8 Å drawn. The Mn1 atoms are octahedrally coordinated by 4 Mn2 and 4 Sb neighbours whereas the Mn2 atoms have only 5 close neighbours: 4 Mn1 and 1 Sb, which probably accounts for their larger moment. The structure refinements have shown that in spite of the abrupt 0.4% reduction in the length of the c-axis at T_{ms}, the only bond lengths which change by more than 0.15% are the four between Mn1 and Sb, and the single one between Mn2 and Sb. These all decrease by ≈0.4% on cooling through the transition whereas all the other bond lengths, including the short bonds (2.758 Å) from Mn1 to Mn2 shown as dashed lines in the figure, decrease by less 0.15%. The contraction of the c-axis in the FI–AF transition can not therefore be caused by an decrease in size of just one of the Mn atoms, it must be due to increased participation in the bonding bands of the 3d zy and zx orbitals associated with Mn1 and the $3z^2 - r^2$ orbitals associated with Mn2.

It can be seen from figure 5 that the Mn1 and Mn2 atoms lie in separate (00l) planes: they are ferromagnetically aligned within these planes. The sequence of planes along the c-axis is

$$Mn1_0 - Mn2_z - (Mn2_{1-z} - Mn1_1 - Mn2_{1+z}) - Mn2_{2-z} - \cdots.$$

The subscripts refer to the value of z and the group contained within the bracket represents the basic magnetic unit, within which the Mn1 and Mn2 moments are oppositely aligned in both the FI and AF phases. In the FI phase the magnetic units repeat along the c axis whereas in the antiferromagnetic state neighbouring units are oppositely oriented.

In the exchange inversion model for a transition from FI to AF order [11] the exchange interaction between adjacent magnetic units changes sign when their separation reaches a

certain value. The transition at T_{ms} occurs when the contraction of the c-axis on cooling causes the inter-unit distance to fall below this critical value. However because of the itinerant nature of the magnetic electrons the exchange interaction driving the transition must depend on details of the band structure for which calculations predict that the Fermi level falls between two peaks in the density of states. The shortest Mn–Mn distance is between Mn1 and Mn2 atoms within the same magnetic unit and the band structure calculations [6] show that it is hybridization between electron orbitals of these Mn1 and Mn2 atoms which is responsible for the strong direct antiferromagnetic exchange within the triple layer magnetic unit. It is significant that neither this bond length nor the sign of this exchange interaction change in the FI to AF transition. The same electronic structure calculations suggest that the coupling between adjacent units takes place via a small direct exchange or by indirect exchange involving the Sb atoms. The two possible paths the indirect exchange can take are $\simeq$125° $Mn2_z$–Sb_{1-z}–$Mn1_1$ or 90° $Mn2_z$–Sb_{1-z}–$Mn2_{1-z}$. The present results show that the only significant changes in bond length at T_{ms} are in the Mn1–Sb and the Mn2–Sb distances thus establishing the 125° path as the predominant interlayer exchange interaction.

In figure 4 the moments determined in the experiment are compared with the sum of the Mn1 and Mn2 moments determined from the magnetization measurements. The temperature dependence of the magnetization can by no means be fitted by a Brillouin curve. It does not appear to be saturated at the FI–AF transition ($T_{ms}/T_C = 0.3$) and the moments measured in the AF phase below T_{ms} indicate that the effective magnetization per formula unit continues to rise below T_{ms}. The results give very little evidence for any anomalous change in the Mn2 moment at T_{ms} in the alloy with $x = 0.1$. They suggest that the Mn2 moment increases more or less continuously between 200 and 4 K whereas the Mn1 moment appears to decrease below T_{ms}. There is some evidence that this decrease may be due to antiparallel alignment of the Co and Mn1 moments. The moments obtained by [3] for $Mn_{1.8}Co_{0.2}Sb$ lie systematically below our present values suggesting that increasing cobalt content reduces the moment at both sites even though it only enters the Mn1 site.

The magnetization distribution around the Mn2 atoms in both phases has approximately spherical symmetry characteristic of a nearly half filled 3d band. The magnetic electrons around the Mn1 atoms in the antiferromagnetic phase have essentially complete t_{2g} symmetry. On heating into the ferrimagnetic phase the increase in the Mn1 moment appears to be associated with unpairing of electrons in the $d_{3z^2-r^2}$ e_g orbitals.

Narrow well separated bands for the Mn2 atoms, one above and one below the Fermi level, will explain the near spherical symmetry of the magnetization distribution of these atoms which was found in both the FI and AF states. The continuing increase in Mn2 moment on cooling through the transition must be due to diminishing overlap between the narrower bands of the AF state. The magnetization of the Mn1 atoms is more complex because their bands are broader and those of the two spin states overlap strongly, the presence of cobalt in these sites can consequently lead to important changes. Taken in conjunction with the band structure calculations, the present results suggest that the Mn1 magnetization in the AF phase is due to unfilled antibonding states with t_{2g} symmetry. In the FI state additional band broadening must lead to increasing overlap between this band and bands based on the $3z^2 - r^2$ non-bonding orbitals.

5. Conclusions

The abrupt 0.4% change in the c axis parameter at T_{ms} does not lead to the significant change in atomic volume which would be expected if the magnitude of one of the Mn moments were to increase abruptly on entering the AF phase as previously reported [3]. In fact the change in cell volume is negligible <0.05% suggesting that the magnitude of the Mn moments do not change in the transition. The invariance of the moments has been directly confirmed by combining polarized and unpolarized neutron diffraction. The results suggest that the anomalous decrease in the c axis parameter at T_{ms} is associated with increased occupation of the Mn1 and Mn2 bonding orbitals which hybridize with Sb. Analysis of the bond lengths above and below T_{ms} shows that the most significant change occurs in the Mn1–Sb and Sb–Mn2 bonds which link the magnetic units whose coupling reverses in the transition. This establishes the 125° Mn1–Sb–Mn2 interlayer path as the predominant exchange interaction determining the type of long range magnetic order.

References

[1] Swoboda T J, Cloud W H, Bither T A, Sadler M S and Jarrett H S 1960 *Phys. Rev. Lett.* **4** 503
[2] Kanomata T and Ido H 1984 *J. Appl. Phys.* **55** 2039
[3] Ohashi M, Yamaguchi Y and Kanomata T 1992 *J. Magn. Magn. Mater.* **104–107** 925
[4] Suzuki T, Kanomata T, Yoshida H and Kaneko T 1990 *J. Appl. Phys.* **67** 4816–7
[5] Suzuki M, Shirai M and Motizuki K 1992 *J. Phys.: Condens. Matter* **4** L33
[6] Wjingaard J H, Haas C and deGroot R A 1992 *Phys. Rev.* B **45** 5395
[7] Kimura A, Suga S, Shishidou T, Imada S, Muro T, Park S Y, Miyahara T and Kanomata T 1997 *Phys. Rev.* B **56** 6021
[8] Baranov N V, Khrulev Yu, Bartashevich M I, Goto T and Aruga-Katori A 1999 *J. Alloys Compounds* **292** 11
[9] Bartashevich M I, Goto T, Zemlyanski S V, Hilscher G and Michor H 2002 *Physica* B **318** 198
[10] Alperin H A, Brown P J and Nathans R 1963 *J. Appl. Phys.* **34** 1201
[11] Kittel C 1960 *Phys. Rev.* **120** 335